Inorganic Chemistry

Article

pubs.acs.org/IC

^{27}Al and ^{29}Si Solid-State NMR Characterization of Calcium-Aluminosilicate-Hydrate

Xiaolin Pardal,[†] Francine Brunet,[‡] Thibault Charpentier,[‡] Isabelle Pochard,*[,†] and André Nonat[†]

[†]Laboratoire Interdisciplinaire Carnot de Bourgogne, UMR 5209 CNRS-Université de Bourgogne, 9 Avenue Savary, BP 47 870, F-21078 Dijon Cedex, France

[‡]CEA, IRAMIS, SIS2M, LSDRM, UMR 3299 SIS2M CEA-CNRS, F-91191 Gif-sur-Yvette, France

ABSTRACT: Calcium silicate hydrate (C-S-H) is the main constituent of hydrated cement paste and determines its cohesive properties. Because of the environmental impact of cement industry, it is more and more common to replace a part of the clinker in cement by secondary cementitious materials (SCMs). These SCMs are generally alumina-rich and as a consequence some aluminum is incorporated into the C-S-H. This may have consequences on the cohesion and durability of the material, and it is thus of importance to know the amount and the location of Al in C-S-H and what the parameters are that control these features. The present paper reports the ^{29}Si and ^{27}Al MAS NMR analyses of well-characterized C-A-S-H samples (C-S-H containing Al). These samples were synthesized using an original procedure that successfully leads to pure C-A-S-H of controlled compositions in equilibrium with well-characterized solutions. The ^{27}Al MAS NMR spectra were quantitatively interpreted assuming a tobermorite-like structure for C-A-S-H to determine the aluminum location in this structure. For this purpose, an in-house written software was used which allows decomposing several spectra simultaneously using the same constrained spectral parameters for each resonance but with variable intensities. The hypothesis on the aluminum location in the C-A-S-H structure determines the proportion of each silicon site. Therefore, from the ^{27}Al NMR quantitative results and the chemical composition of each sample, the intensity of each resonance line in the ^{29}Si spectra was set. The agreement between the experimental and calculated ^{29}Si MAS NMR spectra corroborates the assumed C-A-S-H structure and the proposed Al incorporation mechanism. The consistency between the results obtained for all compositions provides another means to assess the assumptions on the C-A-S-H structure. It is found that Al substitutes Si mainly in bridging positions and moderately in pairing positions in some conditions. Al in pairing site is observed only for Ca/(Si+Al) ratios greater than 0.95 (equivalent to 4 mmol.L^{-1} of calcium hydroxide). Finally, the results suggest that penta and hexa-coordinated aluminum are adsorbed on the sides of the C-A-S-H particles.

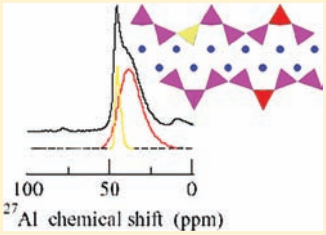

1. INTRODUCTION

Calcium silicate hydrate (generally called C-S-H) is the main constituent of the hydrated cement[1] paste and is responsible for its cohesive properties. It is the most common nano material since several hundred millions tons are produced every year worldwide. Although it is a very common material, its structure at different length scales is still under debate. It is now generally agreed that C-S-H has a layered structure close to that of the mineral tobermorite. Both of them are based on a calcium plane flanked on each side by linear silicate "dreierketten" chains[2] (see Figure 1), as demonstrated by ^{29}Si MAS NMR measurements.[3−6] In these silicate chains, the silicate tetrahedra coordinating calcium atoms of the calcium plane are named pairing tetrahedra whereas the silicate tetrahedra binding two pairing tetrahedra are called bridging tetrahedra. Contrary to tobermorite which has a Ca/Si stoichiometry close to 0.7 corresponding to quasi infinite silicate chains, the stoichiometry of C-S-H varies; it increases from 0.66 to around 2 when the calcium hydroxide activity in equilibrium solution increases. This variation in stoichiometry occurs according to two main mechanisms:

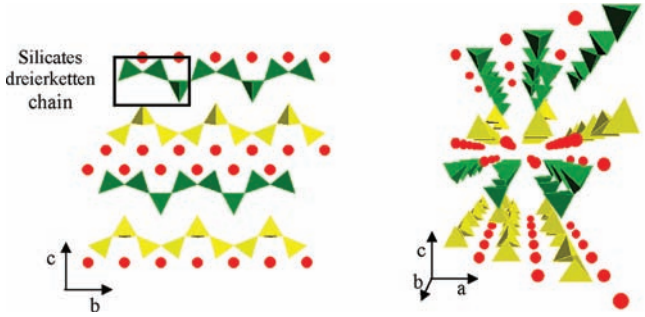

Figure 1. Scheme of the tobermorite structure. Red circles, Ca atoms; yellow and green tetrahedra, silicate tetrahedra.

- the disappearance of bridging tetrahedra in the dreierketten silicate chains which has been extensively studied by ^{29}Si MAS NMR,[3−6]
- the deprotonation of the silanol binding bonds of the bridging and end of chains of silicate tetrahedra which are then compensated by calcium cations.

Received: September 30, 2011
Published: January 25, 2012

   dx.doi.org/10.1021/ic202124x | *Inorg. Chem.* 2012, 51, 1827−1836

Because of the environmental impact of cement industry and its consequences on global warming (the production of 1 ton of clinker emits about 1 ton of CO_2) it is more and more common to replace a part of the clinker in cement by secondary cementitious materials (SCMs), in particular industrial by-product such as blast furnace slag and fly ash (blended cement). These SCMs are much calcium poorer and alumina richer than clinker, and as a consequence the calcium to silicate ratio of C-S-H is lower and some aluminum is incorporated into the C-S-H. It is important to know the amount and the location of Al in C-S-H and what the parameters are controlling them because the presence of Al may have consequences on the cohesion and durability of the material. From the durability point of view, Al containing C-S-H (C-A-S-H) can act as an aluminum reservoir which may lead, in the case of an external sulfate attack by groundwater, for example, to a delayed ettringite [Ettringite is a hydrated calcium trisulfoaluminate, $Ca_6Al_2(SO_3)_3OH_{12}\cdot 26H_2O$] formation (DEF) which is a severe concrete pathology. In addition, the substitution of one Si^{IV} by one Al^{III} introduces one negative permanent charge in a similar way than in clays, which is important from the point of view of cohesion of cement paste. It was shown that, in the early age, the cohesion of hydrated cement paste is due to attractive electrostatic forces between charged C-S-H particles.[7−9] The permanent charge brought by the Si−Al substitution could thus influence these electrostatic cohesion forces.

Many studies have been devoted to the Al incorporation in C-S-Hs. Kalousek[10] was the first to demonstrate that aluminum may enter the structure of tobermorite. Many of the studies were carried out using ^{27}Al MAS NMR or/and ^{29}Si MAS NMR. ^{27}Al MAS NMR has often been used to characterize materials where Al occurs in several environments for it is possible to differentiate the various coordinations of aluminum by their different isotropic chemical shifts. The chemical shifts of ^{27}Al are in the range 50−100 ppm for the tetrahedral, 10−20 ppm for the octahedral, and 30−40 ppm for the pentahedral sites. ^{29}Si MAS NMR has also proven to be a very useful tool for the characterization of the different types of SiO_4 silicon tetrahedra according to their connectivity such as Q^1 dimers, Q^2 bridging (Q^2_B) or pairing (Q^2_P) groups, and Q^3 branching sites. The isotropic chemical shift (δ) is the most informative parameter because it reflects the structural surroundings of a silicon atom. It is well-known that the increase of polymerization of the silicon tetrahedra leads to a lower frequency chemical shift, and the presence of aluminum instead of adjacent silicon to a given Si site produces a higher frequency shift of about 3−5 ppm.[11]

Several authors have investigated the incorporation of aluminum in tobermorite and C-S-H by means of ^{27}Al and ^{29}Si high-resolution Magic Angle Spinning (MAS) spectroscopy.[12−25] However, these studies did not allow to quantify properly the different occupancies of Al in C-A-S-H or to relate them to the chemical conditions. The first reason comes from the chemistry of the samples which is generally not well-controlled. Either the synthesized C-A-S-H is mixed with other aluminates phases or alkali salts are employed[14,24] which confuse the results: it is indeed possible that sodium plays an important role for the Al^{III} for Si^{IV} substitution.[18] Also, numerous studies are devoted to cement pastes instead of pure phases.[12,20−22,25,26] The second reason comes from the fact that quantitative results about the Al speciation in C-A-S-H are poor because the decompositions of ^{27}Al or ^{29}Si NMR spectra have never been really successful despite a few attempts.[13,20,22] In these works, ^{29}Si MAS NMR spectra were decomposed on the basis of an ad hoc assumption about the C-A-S-H structure, which, however, could not be confirmed independently.

In this situation, it is necessary to study C-A-S-H in a range of stoichiometries and under various equilibrium conditions corresponding to different Al chemical potentials. Here we have used a procedure described previously[27] which leads to C-A-S-H samples of controlled composition in equilibrium with a well characterized solution. The present paper deals with the ^{29}Si and ^{27}Al MAS NMR analyses of these well-characterized samples to quantify the incorporation of aluminum into C-S-H and to localize these aluminum atoms in the C-S-H structure. Note that ^{29}Si spectra alone cannot provide reliable results without a precise idea of the C-A-S-H structure, because the resonance peaks in the ^{29}Si spectra overlap which makes their interpretation difficult. Hence, in this work a better method was employed which consists in decomposing first the ^{27}Al spectra so that a working hypothesis for the aluminum location in the C-A-S-H can be made. To this end, we used an in-house written software which allows one to decompose several spectra simultaneously using the same constrained spectral parameters for each resonance but with variable intensities. Indeed, it is often difficult to separate several ^{27}Al sites whose isotropic chemical shifts spread all within about 10−20 ppm and are smaller than the quadrupolar broadening of the lines (which exists only for nuclei with spin $I > 1/2$, such as ^{27}Al). In this work, ^{27}Al spectra have first been interpreted on the assumption of a tobermorite-like structure for C-A-S-H to determine the aluminum location. From the latter, the proportion of each silicon site can then be obtained. For instance, the proportion of Si Q^3(1Al) is obviously equal to the proportion of Al in Q^3 position. Therefore for each sample, from the quantitative analysis of its ^{27}Al NMR spectrum and its chemical composition, the intensity of each resonance line in the ^{29}Si spectra can been set. The agreement between the experimental and calculated ^{29}Si spectra proves the assumed C-A-S-H structure. Consistency between the results obtained for all compositions provides another means to assess the assumptions on the C-A-S-H structure and proposed Al incorporation mechanism. All these experimental results will be useful to develop a thermodynamic model describing C-A-S-H in equilibrium with electrolytic solutions. This latter point will be developed in a forthcoming paper.

2. EXPERIMENTAL SECTION

2.1. Synthesis of Samples. The Al-substituted-C-S-H (C-A-S-H) samples were synthesized by a three-step procedure described in detail elsewhere.[27] Solid samples with different Al/Si ratios can be obtained. The pH of the C-A-S-H suspensions was measured and then the suspensions were filtered to separate the liquid and the solid phases. The filtrates were analyzed by Inductive Coupled Plasma-Optical Emission Spectroscopy (ICP-OES) to determine the calcium, silicon and aluminum concentrations. The solids were washed twice with an alcohol−water mix, and once with pure alcohol. The alcohol was removed by gently pumping for 5 days and the solid samples were finally stored in a desiccator containing a reservoir of calcium hydroxide to avoid carbonation of samples. The solids were analyzed by X-rays Diffraction (XRD), Energy Dispersive X-ray Spectrometry using a Transmission Electronic Microscope (EDS-TEM), and solid state NMR spectroscopy. The XRD and EDS results have been reported previously.[27]

Two C-A-S-H samples series of different Al/Si ratios were studied: C-A-S-H with Ca/(Al+Si) = 0.70 and C-A-S-H with Ca/(Al+Si) = 0.95 named C-A-S-H 0.70 and C-A-S-H 0.95, respectively. To explore

dx.doi.org/10.1021/ic202124x | Inorg. Chem. 2012, 51, 1827−1836

the evolution of the Al/Si ratio with the increase of the calcium hydroxide concentration a series of samples (named C-A-S-H in $Ca(OH)_2$) was obtained by equilibrating C-A-S-H (Al/Si = 0.19, Ca/(Al+Si) = 0.70) in different calcium hydroxide solutions at a weight concentration of 2 $g{\cdot}L^{-1}$. The initial calcium hydroxide concentrations were 0 mM, 5.53 mM, 10.92 mM, 15.17 mM, 19.05 mM, and 21.63 mM.

2.2. Nuclear Magnetic Resonance. The solid-state NMR experiments were performed on a Bruker Avance 300WB (7.05 T) spectrometer operating at a frequency of 59.59 MHz for ^{29}Si and on a Bruker Avance 500WB (11.72 T) operating at a frequency of 130.4 MHz for ^{27}Al. For both nuclei, a 4 mm o.d. Bruker CPMAS probe was used with a spinning frequency of 12.5 kHz. ^{27}Al spectra were recorded, with a Single Pulse Excitation (SPE) using a short pulse length (1 μs) to obtain quantitative results, and a recycle delay of 1 s (the RF field strength was 41 kHz and the tip angle was $\pi/12$). ^{1}H decoupling was found not to be necessary as not modifying the spectra. ^{27}Al chemical shifts were referenced using $AlCl_3{\cdot}6H_2O$ 1 M in solution as an external reference (0 ppm). ^{29}Si spectra were recorded using a 90° pulse length of 5.7 μs with a recycle delay of 60 s to yield quantitative spectra. To obtain spectra with a good signal-to-noise ratio, experimental times of about 17 h were necessary. ^{29}Si chemical shifts were referenced using tetrakis(trimethylsilyl)silane as the external reference (two resonances at −9.9 ppm and −135.3 ppm with respect to liquid tetramethylsilane). Complementary ^{27}Al MAS and MQMAS experiments were also performed on a Bruker Avance 800WB (18.8 T) spectrometer using 3.2 mm o.d. Bruker CPMAS probe at a spinning frequency of 20 kHz.

2.3. Decomposition of the Spectra. All ^{27}Al and ^{29}Si NMR spectra have been simulated using a software developed by Charpentier.[28,29] This software enables several NMR spectra to be decomposed simultaneously using the same spectral parameters for each individual component across the collected data. As an additional feature, the relative intensity of some components can be fixed to agree with the proportion of the corresponding sites in the structural model of the material.

For ^{29}Si spectra, choosing each component as a mixture of a Gaussian and a Lorentzian function was found to yield the best results:

$$f(\nu) = \sigma G(\nu - \delta, g_b) + (1 - \sigma)L(\nu - \delta, l_b) \quad (1)$$

The spectral parameters are the isotropic chemical shift, δ, the Gaussian broadening, g_b (the Lorentzian broadening, l_b, is fixed so that $G(\nu, gb)$ and $L(\nu, gb)$ have the same width at the middle height), and the Gaussian to Lorentzian ratio, σ ($0 \le \sigma \le 1$).

For ^{27}Al spectra, the shape of the resonances was found to be characteristic of a distribution of both the local electric field gradient (as characterized by the quadrupolar coupling constant C_Q and the quadrupolar asymmetry parameter η) and the isotropic chemical shift δ. On the basis of recent works,[30−32] the software uses the Gaussian Isotropic Model (GIM)[33,34] for the distribution of the electric field gradient, here denoted $\Pi(C_Q, \eta; \sigma_Q)$, and a normal (Gaussian) distribution for the isotropic chemical shift $G(\delta; g_b)$ to simulate the MAS spectrum $f(\nu)$ as follows

$$f(\nu) = \int d\delta\, dC_Q\, d\eta \times I(\nu - \delta; C_Q, \eta) \times \Pi(C_Q, \eta; \sigma_Q) \times G(\delta; g_b) \quad (2)$$

σ_Q is the only parameter that characterizes the GIM distribution.[33,34] $I(\nu; C_Q, \eta)$ are precalculated (i.e., theoretical) MAS spectra according to the parameters C_Q and η and incorporating other experimental parameters (magnetic field, spin rate, rf pulse, etc.). The Gaussian Isotropic Model (GIM) has already been shown to provide good lineshapes for the analysis of the Al MAS NMR spectra in C-S-H.[32,35]

3. RESULTS AND DISCUSSION

3.1. Chemical analyses. The ionic composition (pH and silicon, calcium and aluminum concentrations) of the equilibrium solutions, stoichiometry of C-A-S-H in terms of Al/Si and Ca/(Al+Si) ratios, and crystalline phases present for all the studied samples are reported in Tables 1 and 2.

Table 1. Chemical Data for the Series "C-A-S-H 0.70" and "C-A-S-H 0.95"

Al/Si ± 0.01	Ca/(Al+Si) ± 0.02	[Si] (mM)	[Ca] (mM)	[Al] (mM)	pH ± 0.05	phase
			C-A-S-H 0.70			
$0.12^{Si,Al}$	0.71	0.30	1.81	0.14	11.90	C-A-S-H
0.13^{Si}	0.71	0.23	2.00	0.20	11.95	C-A-S-H
0.16^{Si}	0.71	0.10	2.36	0.54	12.05	C-A-S-H
$0.18^{Si,Al}$	0.73	0.04	3.15	1.42	12.05	C-A-S-H
$0.19^{Si,Al}$	0.73	0.02	4.40	2.61	12.20	C-A-S-H
			C-A-S-H 0.95			
$0.11^{Si,Al}$	0.94	0.06	3.21	0.38	12.20	C-A-S-H, calcite[a]
0.16^{Al}	0.94	0.02	4.02	1.61	12.30	C-A-S-H, calcite[a]
0.34^{Al}	1.01	0.01	4.73	2.90	12.15	no analysis

^{Si}Si samples analyzed by ^{29}Si NMR. ^{Al}Al samples analyzed by ^{27}Al NMR. [a]Traces of calcite phase were detected.

Table 2. Chemical Data for the C-A-S-H in $Ca(OH)_2$ Series (C-A-S-H 0.70 (Al/Si = 0.19) Equilibrating in Calcium Hydroxide Solutions (C-A-S-H Weight Concentration = 2 $g{\cdot}L^{-1}$))[a]

initial $[Ca(OH)_2]$ (mM)	[Si] (mM)	[Ca] (mM)	[Al] (mM)	pH ± 0.05	phase
0.00	0.36	0.69	0.08	11.25	C-A-S-H
5.53^{Si}	0.16	3.59	0.31	12.10	C-A-S-H
10.92^{Si}	0.02	5.25	0.36	12.40	C-A-S-H, AFm
15.17	0.02	7.25	0.12	12.60	C-A-S-H, AFm
19.05^{Si}	0.01	9.79	0.04	12.70	C-A-S-H, AFm
21.63	0.01	11.98	0.02	12.80	C-A-S-H, AFm

[a]All the samples have been analyzed by ^{27}Al NMR. ^{Si}Si samples analyzed by ^{29}Si NMR. AFm: tetracalcium hemi carboaluminate hydrate $C_4Al_2(OH)_{13}(CO_3)_{0.5}{\cdot}11H_2O$.

In Table 1, the reported Al/Si and Ca/(Al+Si) ratios in the C-A-S-H have been determined by depleting the quantities of Al, Ca, and Si in the equilibrium solution (determined by ICP-OES) to the initial amounts of Al, Ca, and Si coming from the $Ca_3Al_2O_6$ hydration solution and the added C-S-H.[27] In the C-A-S-H 0.95 series and despite the observation of traces of calcite by XRD analysis, the Ca/(Al+Si) ratio has been calculated in the same way because the amount of calcite estimated by the XRD analysis is very low. The XRD patterns reported in ref 27 show that C-A-S-H samples exhibit a tobermorite-like structure without noticeable modification compared to C-S-H. EDS (TEM) analyses presented in a previous work[27] showed that all samples are free of Al amorphous gel and that the C-A-S-H phase is homogeneous in composition.

3.2. ^{27}Al NMR Results. *3.2.1. ^{27}Al NMR Spectra.* The samples analyzed by ^{27}Al NMR are mentioned with the superscript ^{Al} in Tables 1 and 2, and the corresponding spectra are presented below. The intensities of the spectra depicted in Figures 2 and 3 are normalized with respect to the same sample mass to be reliable. The spectra in Figures 2 and 3 show

dx.doi.org/10.1021/ic202124x | Inorg. Chem. 2012, 51, 1827−1836

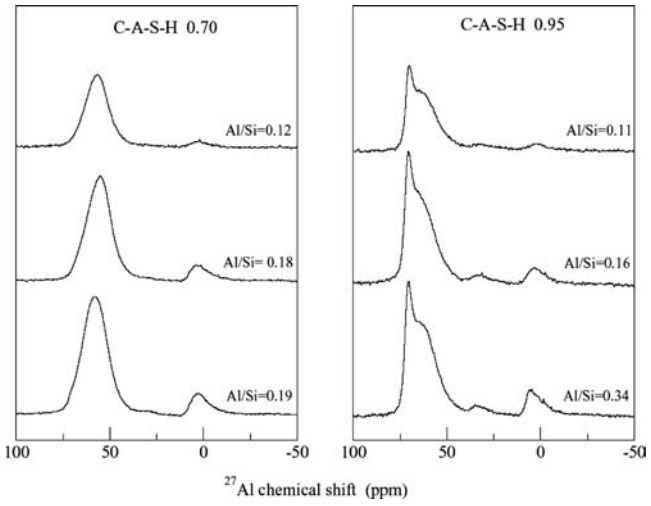

Figure 2. Experimental ^{27}Al MAS NMR spectra acquired at 11.72 T (see section 2.2 for details). Left panel: C-A-S-H 0.70; right panel: C-A-S-H 0.95. The Al/Si ratio of each sample is indicated on the spectra (see Table 1).

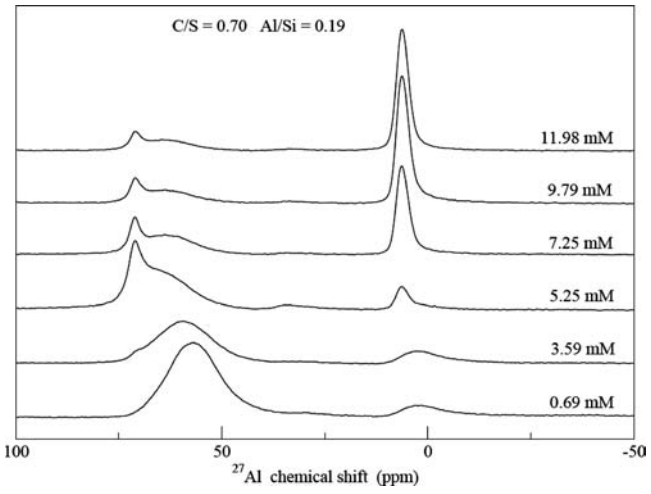

Figure 3. Experimental ^{27}Al MAS NMR spectra acquired at 11.72 T (see section 2.2 for details) for C-A-S-H 0.70 of Al/Si = 0.19 in $Ca(OH)_2$ at different concentrations (see Table 2). $Ca(OH)_2$ concentrations at equilibrium in mM; from bottom to top: 0.69; 3.59; 5.25; 7.25; 9.79; 11.98.

resonances in the regions 70−55 ppm, 30 ppm and 2−5 ppm corresponding to aluminum atoms in coordination 4, 5, and 6, respectively in good agreement with literature data.[13,24,36] A supplementary narrower resonance peak is visible in the hexa-coordinated region for $[Ca(OH)_2] \geq 3.59$ mM in the C-A-S-H in $Ca(OH)_2$ series (Figure 3). The intensity of this resonance increases with the $Ca(OH)_2$ concentration. XRD results show the presence of calcium carboaluminate in all samples.[27] Therefore, this resonance does not originate from a species in the C-A-S-H phase but is characteristic of a calcium carboaluminate phase.

In the tetra-coordinated region (50−70 ppm), two resonances are readily seen: a very broad resonance near 60−70 ppm in all spectra and a narrow resonance near 72 ppm in some samples (C-A-S-H 0.95 and C-A-S-H in $Ca(OH)_2$ for $[Ca(OH)_2] \geq 3.59$ mM). It is generally agreed that the former broad resonance corresponds to tetra-Al in the C-A-S-H structure. Here, we also attributed the latter resonance to tetra-Al in the C-A-S-H structure. One would perhaps be drawn to ascribe it to another amuminosilicate phase, strätlingite ($Ca_2Al_2SiO_2(OH)_{10}\cdot 3H_2O$) in which Al occurs in both tetrahedral and octahedral environments. This was observed in ref 26 where strätlingite precipitated besides C-A-S-H. However, strätlingite is a well-crystalline phase, readily seen by X-ray diffraction, which was however not found in our samples. Moreover, the resonance of tetrahedral Al in strätlingite is expected to occur at 62 ppm,[37] that is, 10 ppm below the chemical shift observed here. This gap is sufficiently significant to ensure that the narrow resonance at 72 ppm is not due to strätlingite, which is confirmed by XRD as discussed above.

Considering the broad resonance in the tetrahedral region, a significant shift of the maximum from 60 to 70 ppm is observed across the sample series. The question arises whether this resonance actually hides one or two distinct contributions. Complementary solid-state NMR experiments (MAS and MQMAS) were therefore performed at higher field on a Bruker Avance 800WB spectrometer. The results as depicted in Figures 4 and 5 confirm that the width of the line is reflective of

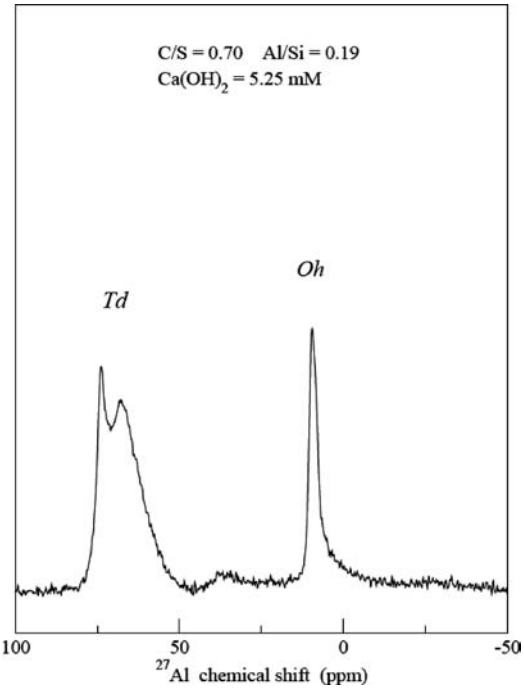

Figure 4. Experimental ^{27}Al MAS NMR spectra of C-A-S-H 0.70 (Al/Si = 0.19) in 5.25 mM of $Ca(OH)_2$ acquired at 18.8 T (see section 2.2 for details).

a broad continuous distribution of resonances from 60 to 70 ppm; thus, the hypothesis of two distinct resonances can be rejected. Note that the signal-to-noise ratio in Figure 4 is lower than in Figure 3 because of the reduced sample volume that could be analyzed at 18.8 T. In agreement with these observations, the decomposition and quantitative analyses of all the spectra were performed assuming a single distribution of resonances, eq 2, underlying the broad line in the 60−70 ppm range.

3.2.2. ^{27}Al NMR Spectra Decomposition. According to the discussion of the previous section, all C-A-S-H spectra were decomposed into five individual resonances. Three broad components were observed in all samples denoted Al[IV]-a (AlO_4), Al[V] (AlO_5), and Al[VI]-a at about 60−70, 30, and 5

dx.doi.org/10.1021/ic202124x | Inorg. Chem. 2012, 51, 1827−1836

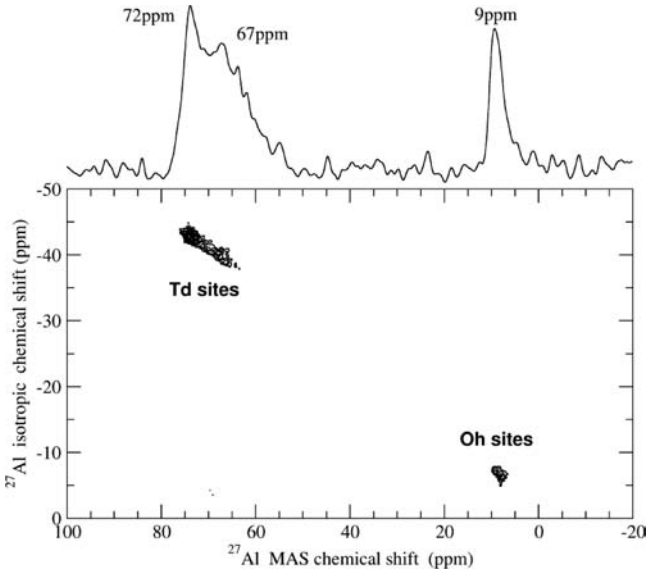

Figure 5. ^{27}Al MQ MAS NMR spectrum of the same sample as in Figure 4. See section 2.2 for NMR acquisition details.

ppm, respectively. Two other narrow lines were introduced in our model: Al[IV]-b at around 72 ppm and Al[VI]-b at around 2 ppm. Figure 6 shows details of the decomposition for two

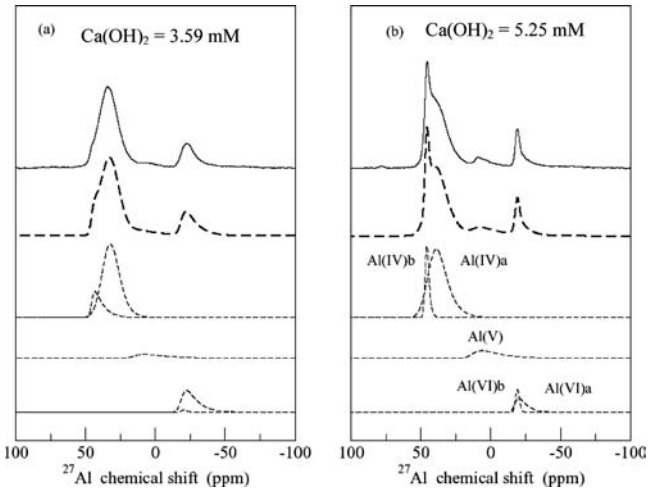

Figure 6. ^{27}Al MAS NMR experimental (11.72 T) and simulated (see section 2.3 for details) spectra for C-A-S-H 0.70 (Al/Si = 0.19) in (a) [Ca(OH)$_2$] = 3.59 mM; (b) [Ca(OH)$_2$] = 5.25 mM. The experimental spectra (full line) are taken from Figure 3. The simulated spectra (bold dashed lines) nicely match the experimental spectra in both cases. The calculated resonance peak of each of the five kinds of aluminum is also depicted (dashed lines). The simulated spectra in (a) and (b) are the sums of these 5 resonances.

representative C-A-S-H samples. Excellent agreement between simulation and experiment was obtained for all spectra. Table 3 reports the NMR parameter ranges of the five resonances observed across the sample series. The order of magnitude of the relative ratio between the isotropic chemical shift and quadrupolar broadening as obtained from the fit of the MAS spectra could be assessed with the analysis (not shown here) of the MQMAS spectrum (Figure 6).

3.2.3. Quantitative Analysis. As mentioned in paragraph 3.2.1., the Al[VI]-b resonance characterizes a calcium

Table 3. Isotropic Chemical Shift (δ, ppm), Gaussian Broadening (g_b, ppm), and GIM Parameters (σ_Q, MHz) of Each Resonance for the Simulation of the ^{27}Al MAS Spectra[a]

	δ (ppm)	g_b (ppm)	σ_Q (MHz)	C_Q (MHz)
Al[IV]-a	60.3−69.2	5.0−5.9	1.5−2.1	3.2−4.4
Al[IV]-b	71.0−72.0	0.8−1.2	1.0−2.0	2.0−4.2
Al[V]	39.0−41.0	3.5	3.1−3.4	6.4−6.8
Al[VI]-a	6.5−8.5	1.8−2.3	2.0−2.6	4.2−5.5
Al[VI]-b	6.5−8.5	1.1−1.5	0.8−1.2	1.7−2.5

[a]The calculated mean value of the quadrupolar coupling constant (C_Q, MHz) is also listed.

carboaluminate (AFm) phase and was thus not considered for the semiquantitative analyses which concern the C-A-S-H only. Note that the NMR parameters reported in Table 3 agree well with the literature data for AFm: δ = 10.2 ppm and C_Q = 1.3−1.8 MHz in refs 12, 13, 26 and δ = 10.4 ppm and C_Q = 2.2 MHz in ref 35 The proportions of each of the four Al sites in the C-A-S-H are given in Table 4.

Table 4. Proportion (%) of Each Al Site Present in C-A-S-H As Obtained from ^{27}Al MAS NMR Analysis[a]

	Al[IV]-a %	Al[IV]-b %	Al[V] %	Al[VI]-a %
	C-A-S-H 0.70			
Al/Si = 0.19	81	2	5	11
Al/Si = 0.18	80	2	7	11
Al/Si = 0.12	81	0	8	10
	C-A-S-H 0.95			
Al/Si = 0.34	62	19	9	9
Al/Si = 0.16	61	20	10	9
Al/Si = 0.11	63	21	10	6
	C-A-S-H in Ca(OH)$_2$			
Ca(OH)$_2$ = 0.00 mM	83	0	6	11
Ca(OH)$_2$ = 3.59 mM	62	14	6	17
Ca(OH)$_2$ = 5.25 mM	66	15	10	8
Ca(OH)$_2$ = 7.25 mM	60	13	7	18
Ca(OH)$_2$ = 9.79 mM	45	13	9	33
Ca(OH)$_2$ = 11.98 mM	46	10	8	36

[a]See text for details. The octa-Al in the calcium carboaluminate phase (Al[VI]-b) has not been considered. Precision is estimated to ±5%.

The accuracies of the values reported in Table 4 is estimated to about 5%. Results for C-A-S-H in calcium hydroxide >3.59 mM series are less accurate, especially for the Al[VI]-a proportion, because of the great proportion of Al[VI]-b site (about 50%).

The following general trends can be drawn from these data: the proportion of Al[V] is low and remains as low as 5−10% in all samples. Concerning Al[IV]-b, there are around 20% in the samples of C-A-S-H 0.95 and about 10−15% in the samples equilibrated in calcium hydroxide solutions. Al[IV]-b is not present in the samples of the C-A-S-H 0.70 series and in the sample equilibrated in water (C-A-S-H in [Ca(OH)$_2$] = 0.00 mM). Finally, the proportion of the Al[IV]-a site is 80% in the samples of the C-A-S-H 0.70 series, around 62% in the samples of the C-A-S-H 0.95 series and decreases from 83% to 46% with the calcium hydroxide concentration increasing in the samples equilibrated in these solutions.

According to the dreierketten structure of the silicate chain in C-A-S-H, possible Al tetrahedral positions are Q^1, Q^2_P, Q^2_B, and Q^3 (see Introduction for designation). However, Al atoms can

dx.doi.org/10.1021/ic202124x | Inorg. Chem. 2012, 51, 1827−1836

hardly be accommodated at the Q^1 site[12,20,21,24,26,38] which will therefore not be further considered in this study. It is generally agreed that the Al substitution occurs in the bridging tetrahedra. Sun et al.[24] proposed that the Al[IV]-a signal corresponds to Al located in Q^3 positions or in $Q^2_{bridging}$ positions charge-balanced by Ca^{2+} and that Al[IV]-b could correspond to Al also located in $Q^2_{bridging}$ position but charge-balanced by Al[V] and/or Al[VI]. However, the amount of Al[IV]-b does not correlate with that of Al[V] + Al[VI]-a (see Table 4). For instance, in the C-A-S-H 0.70 series, 16−18% of Al[V] + Al[VI]-a are present without any Al[IV]-b, which contrasts with the C-A-S-H 0.95 series which has 19−21% Al[IV]-b but still 16−19% Al[V]+Al[VI]-a.

Furthermore, the MAS and MQMAS NMR experiments performed at high field (800 W B, 18.8 T) demonstrate that the isotropic chemical shift of the Al[IV]-a site is broadly distributed from 60 to 70 ppm. This indicates that the Al[IV]-a resonance should correspond to tetrahedral aluminum in close but slightly different chemical environments. Conversely, the Al[IV]-b site exhibits a narrow distribution (low gb, see Table 3) with an isotropic chemical shift centered on 71−72 ppm. Recent theoretical works[38,39] have shown that even if bridging positions such as Q^3 or Q^2_B are energetically favored for Al, the pairing position Q^2_P is likely to occur as well, especially when the Ca/Si ratio of the C-S-H is increased. In these works, the incorporation of tetracoordinated Al ions in the dreierketten configuration of silicates chains was investigated by ab initio calculations. It is shown that the structure with the lower energy is the one with Al in bridging position Q^3 or Q^2_B .Nevertheless, the difference between the bridging and pairing sites being small (0.17 eV per pentamer unit), these two positions are able to compete even at room temperature.

From all these observations, we propose that the Al[IV]-a species corresponds to Al in bridging positions: Q^3 and Q^2_B possibly charge-balanced by Ca^{2+} as proposed by Sun et al. The existence of several species of very close environment (bridging position) would explain the width of the Al[IV]-a site. Consequently and according to the literature[38,39] the Al[IV]-b resonance would be better assigned to Al in Q^2_p positions, which is compatible with a narrow distribution of isotropic chemical shift as Q^2_p positions are characterized by a well-defined chemical environment. Moreover, this assignment has already been cited in the literature.[14]

According to the present decomposition method of ^{27}Al NMR spectra, an accurate quantification of aluminum species present in the sample was made. Their localization in the different sites of C-A-S-H structure could be suggested assuming a structure based on tobermorite. This hypothesis enables to constrain the prediction of the ^{29}Si NMR spectra decomposition as described in the next section.

3.2.4. Conditions of Al/Si Substitution in Bridging and/or Pairing Positions. From the percentage of aluminum in bridging (Al[IV]-a %) and pairing (Al[IV]-b %) positions, it is possible to calculate the $Al_{bridging}/Si$ and $Al_{pairing}/Si$ ratios. For instance, for the C-A-S-H 0.95 sample with Al/Si = 0.11, Table 4 shows that the Al[IV]-a represents 63% and the Al[IV-b] represents 21% of the total Al (the remaining percentage being the Al[V] and Al[VI]-a). It means that $Al_{bridging}/Si = 0.11 \times 0.63 = 0.07$ and that $Al_{pairing}/Si = 0.11 \times 0.21 = 0.02$. The variation of these two ratios versus the aluminum concentration in the bulk solution for the three series is depicted in Figure 7.

In the case of infinite chain length, Al only substitutes Si in bridging tetrahedra (C-A-S-H 0.70). On the contrary, when the pH is increased and the chain length decreases, both Al in bridging and pairing positions are observed (C-A-S-H 0.95 and C-A-S-H in $Ca(OH)_2$). This is in full in agreement with the ab initio calculation of the Al/Si substitution in dreierketten silicate chains by Manzano et al.[39] The occurrence of Al in pairing position leads to a decrease of the amount of Al in bridging position (easily noticeable for C-A-S-H 0.95). This can be readily understood by the fact that (i) the chains are shorter and there are less occupied bridging positions by Si as well as Al; (ii) as already said, Al−O−Al are not favored therefore, an Al in pairing position hinders an Al in the neighboring bridging position. Nevertheless, the bridging position is always more occupied by Al than the pairing position. Finally, the data for the C-A-S-H in $Ca(OH)_2$ are not fully consistent with the two others series. Actually, the $Al_{pairing}/Si$ joins the curve of the 0.95 series which seems to be reliable with the expected case of high pH, finite chains. But the $Al_{bridging}/Si$ joins the curve of the 0.70 series. One would have expected the C-A-S-H in lime data to be fully consistent with the C-A-S-H 0.95 data as both series account for the same ionic conditions, especially for pH and calcium concentration. Therefore it seems that the samples of C-A-S-H equilibrated in lime solutions have not reached the equilibrium state yet.

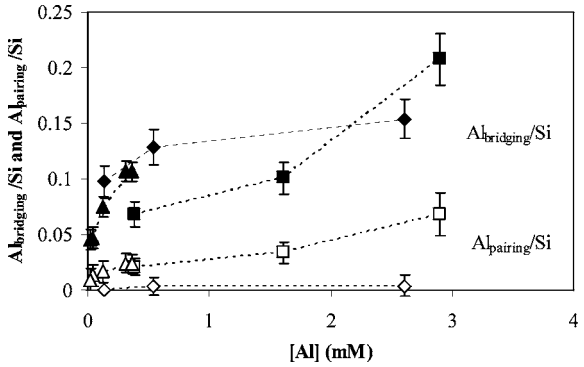

Figure 7. Evolution of the $Al_{bridging}/Si$ (black) and $Al_{pairing}/Si$ (white) ratios with the aluminum bulk concentration. Diamonds: C-A-S-H 0.70; Squares: C-A-S-H 0.95; Triangles: C-A-S-H in lime.

3.3. ^{29}Si NMR Results. *3.3.1. ^{29}Si NMR Spectra.* The samples analyzed are mentioned with the superscript ^{Si} in Tables 1 and 2. As shown in Figure 9, the signal-to-noise ratio is low because of the weak sensitivity of ^{29}Si (small negative γ ; natural abundance 4.7% in addition to a slow longitudinal relaxation) comparatively to ^{27}Al (natural abundance 100% with a rapid quadrupolar relaxation). Identification of the positions of resonance lines is tricky because of the strong overlapping between the ^{29}Si resonances, all located in the chemical shift range between −75 ppm and −95 ppm. The chemical shift of ^{29}Si in silicates depends mainly on the connectivity degree of the silicate tetrahedra.[11] Based on the hypothesis of a tobermorite-like structure for C-A-S-H, four connectivity degrees are possible for the silicate tetrahedra.[40] If a silicate gets one straight neighbor aluminate, it is noted as $Q^n(1Al)$ and the corresponding ^{29}Si chemical shift will move to higher frequency by 3−5 ppm.[11] The same trend occurs if a silicate gets two aluminate neighbors but the chemical shift of the $Q^n(2Al)$ ^{29}Si will move to higher frequency by about 10 ppm. Considering all these possibilities, it appears quickly that the decomposition of these ^{29}Si spectra into more than three contributions without any restrains is not conceivable, even imposing chemical shift range for each different contribution.

dx.doi.org/10.1021/ic202124x | Inorg. Chem. 2012, 51, 1827−1836

3.3.2. ^{29}Si NMR Spectra Decomposition. The ^{29}Si NMR spectra can be a priori calculated according to the location and amount of aluminum in the C-A-S-H as obtained from the ^{27}Al NMR analyses and with the hypothesis of a dreierketten structure for the aluminosilicate chains. One also needs the actual amounts of aluminum and silicon in each sample. These are readily obtained from the chemical analyses of the samples. The ^{29}Si experimental spectra have been fitted using the calculated intensities as constants (just scaled by an overall factor adjusted by the program to fit the spectrum area) and by allowing the NMR parameters values in eq 1 of each resonance to vary in meaningful ranges given in Table 5.

Table 5. Intervals for Chemical Shift (δ, ppm), Gaussian Broadening (g_b, ppm), and Gaussian to Lorentzian Ratio (σ) Used in the Simulation of the ^{29}Si MAS Spectra

	δ (ppm)	g_b (ppm)	σ
$Q^2_B(1Al)$	[−77.2 ↔ −76.0]	[1.0 ↔ 1.5]	[0.0 ↔ 0.6]
Q^1	[−80.0 ↔ −79.2]	[0.7 ↔ 1.2]	[0.0 ↔ 0.6]
$Q^2_P(1Al)$	[−82.0 ↔ −81.0]	[1.3 ↔ 2.2]	[0.0 ↔ 0.6]
Q^2_B	[−83.5 ↔ −82.0]	[0.8 ↔ 1.2]	[0.0 ↔ 0.6]
Q^2_P	[−86.0 ↔ −85.0]	[1.0 ↔ 1.3]	[0.0 ↔ 0.6]
Q^3	[−94.0 ↔ −90.0]	[2.0 ↔ 3.0]	[0.0 ↔ 0.8]

Figure 8 is intended to help understand the relationships between the proportion of each type of aluminum and silicon in the structure. These relationships are as follow (all quantities are in percentages):

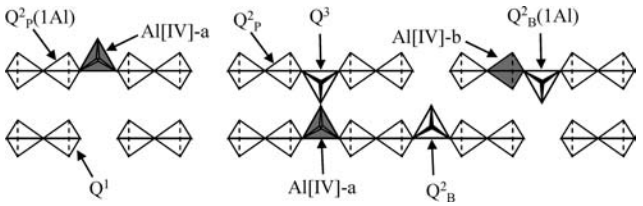

Figure 8. Scheme of the alumino-silicate chains in the C-A-S-H structure.

$$Q^2_B(1Al)\% = Al[IV]\text{-}b\% \quad (3)$$

(the number of Si $Q^2_B(1Al)$ is equal to the number of Al substituting a Si in Q^2_P position)

$$Q^2_P(1Al)\% = 2Al[IV]\text{-}a\% + Al[IV]\text{-}b\% \quad (4)$$

(each Al substituting a Si in Q^3 or Q^2_B position has two Si $Q^2_P(1Al)$ neighbors and each Al substituting a Si in Q^2_P position has a Si $Q^2_P(1Al)$ neighbor)

$$Q^2_B\% + Q^3\% = 1/2Q^2_P\% \quad (5)$$

(according to the drierketten structure, the sum $Q^3\% + Q^2_B\%$ is equal to half of $Q^2_P\%$)

$$Si(total)\% = Q^1\% + Q^2_P\% + Q^2_B\% + Q^2_P(1Al)\% + Q^2_B(1Al)\% + Q^3\% \quad (6)$$

(Si(total)% = 100)

From these conditions and the elemental composition of the samples, intensities of the $Q^2_B(1Al)$ and $Q^2_P(1Al)$ resonances in the ^{29}Si spectra have been calculated (I_{calc} (%) in Table 6). For the spectra decomposition, these intensities were free to vary within 5% from the I_{calc} (%) (leading to I_{exp} (%) in Table 6) in agreement with the accuracy of the quantitative analysis of NMR spectra.

For the C-A-S-H 0.70 series, the $Q^2_B(1Al)$ proportion is close to zero like the Al[IV]-b proportion. Furthermore, in this series, the alumino-silicate chains are quite infinite. This implies that the Q^1 proportion is close to zero. Considering that $Q^1 \approx 0\%$ and $Q^2_B(1Al) \approx 0\%$ and by combining eqs 5 and 6, one finds:

$$Q^2_P\% \approx (100 - Q^2_P(1Al)\%)/1.5 \quad (7)$$

This supplementary relationship allows the calculation of $Q^2_P\%$ for this series (see Table 6). As for the $Q^2_B(1Al)$ and

Table 6. Calculated (I_{calc} (%)) for Q^2_P (C-A-S-H 0.70), $Q^2_B(1Al)$, and $Q^2_P(1Al)$ and Experimental (I_{exp} (%)) Proportions of the Considered Si Sites Present in C-A-S-H after the Quantitative Analysis Obtained from the Simulation of the Experimental Spectra[a]

		Al/Si					$Ca(OH)_2$			C-A-S-H 0.95
		0.19	0.18	0.16	0.13	0.12	3.59 mM	5.25 mM	9.79 mM	Al/Si = 0.11
$Q^2_B(1Al)$	δ (ppm)						−77.0	−77.1	−77.1	−77.0
	I_{calc} (%)	0	0			0	3	3	3	2
	I_{exp} (%)	0	0			0	0	2	3	1
Q^1	δ (ppm)	−79.2	−79.3	−79.6	−79.5	−79.3	−79.3	−79.3	−79.2	−79.2
	I_{exp} (%)	5	6	8	4	4	7	12	13	21
$Q^2_P(1Al)$	δ (ppm)	−81.5	−81.6	−81.9	−81.7	−81.7	−81.9	−81.6	−81.2	−81.2
	I_{calc} (%)	30	29	25	21	19	25	27	19	16
	I_{exp} (%)	29	27	24	22	21	24	31	19	21
Q^2_B	δ (ppm)	−83.0	−82.5	−82.0	−82.7	−82.0	−83.1	−83.0	−82.4	−83.0
	I_{exp} (%)	4	6	5	1	6	6	11	17	13
Q^2_P	δ (ppm)	−85.2	−85.3	−85.4	−85.4	−85.3	−85.7	−85.4	−85.5	−85.2
	I_{calc} (%)	47	47	50	53	54				
	I_{exp} (%)	45	46	49	56	55	41	36	47	39
Q^3	δ (ppm)	−94.5	−94.5	−94.5	−94.5	−92.5	−94.5	−94.4	−94.1	−93.5
	I_{exp} (%)	16	15	14	16	16	23	8	0	5

[a]The experimental chemical shifts (δ ppm) are also listed. Precision of the results presented is estimated to ±5%.

dx.doi.org/10.1021/ic202124x | *Inorg. Chem.* 2012, 51, 1827−1836

$Q^2_P(1Al)$, the intensity of the Q^2_P resonance has been calculated (I_{calc} (%) in Table 6), and this calculated intensity could be within 5% of the calculated values for the spectra decomposition leading to I_{exp} (%) in Table 6.

The individual intensities of the Q^1, Q^2_B, Q^3 resonances for all series and of the Q^2_P resonance for C-A-S-H 0.95 and in $Ca(OH)_2$ cannot be a priori calculated. Hence, these intensities are not set to specific values but adjusted by hand to best fit the experimental spectrum. However, consistency of the results can be checked through eqs 5 and 7. All the resonance intensities (I_{exp} (%)) and chemical shifts (δ ppm) deduced from the decomposition are given in Table 6. The a priori calculated intensity (I_{calc} (%)) for Q^2_P (C-A-S-H 0.70), $Q^2_B(1Al)$, and $Q^2_P(1Al)$ resonances are also listed in this table. Illustrative examples are displayed in Figures 9 and 10. The excellent

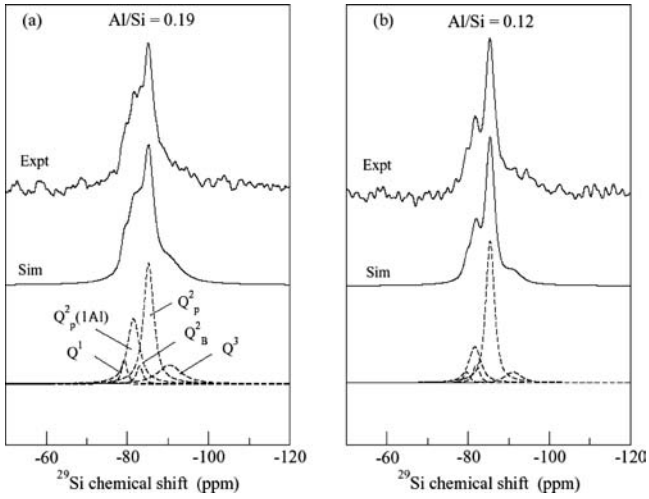

Figure 9. Comparison of the ^{29}Si MAS NMR experimental (acquired at 7.05 T) and simulated spectra for C-A-S-H 0.70. (a) Al/Si = 0.19; (b) Al/Si = 0.12. The simulated spectra (thin solid lines) nicely match the experimental spectra (thick solid lines) in both cases. The calculated resonance peak of each of the five kinds of silicon is also depicted (dashed lines). Each simulated spectrum in (a) and (b) is the sum of these five resonances.

agreement between the experimental and calculated spectra strongly supports the assignment of the different sites for Al derived from the ^{27}Al NMR analyses and the resulting C-A-S-H structure. These results are in strong support of the "tobermorite like" alumino silicate chains in C-A-S-H.

One can easily check that eqs 5 and 7 are nicely fulfilled from the experimental intensities listed in Table 6. As expected, the proportion of Q^1 sites is found negligible in the C-A-S-H 0.70 series for which the alumino-silicate chains are supposed to be infinite. The shortening of the alumino-silicate chains when the calcium hydroxide concentration increases is well illustrated by the increase of the Q^1 site proportion in the C-A-S-H 0.95 and C-A-S-H in $Ca(OH)_2$ series. In the C-A-S-H in $Ca(OH)_2$ series, the Q^3/Q^2_B ratio decreases when the calcium hydroxide concentration is increased as observed for C-S-H gels. This result suggests that the shortening of the chains is achieved by loss of Si atoms in Q^3 position and not loss of Al in Q^2_B position because the proportion of $Q^2_P(1Al)$ remains rather constant. Finally, the proportion of $Q^2_B(1Al)$ is very low indicating a weak proportion of Al in pairing position.

3.4. Penta and Hexa-Coordinated Aluminum. Most of the publications on this topic report that Al[V] and Al[VI]-a

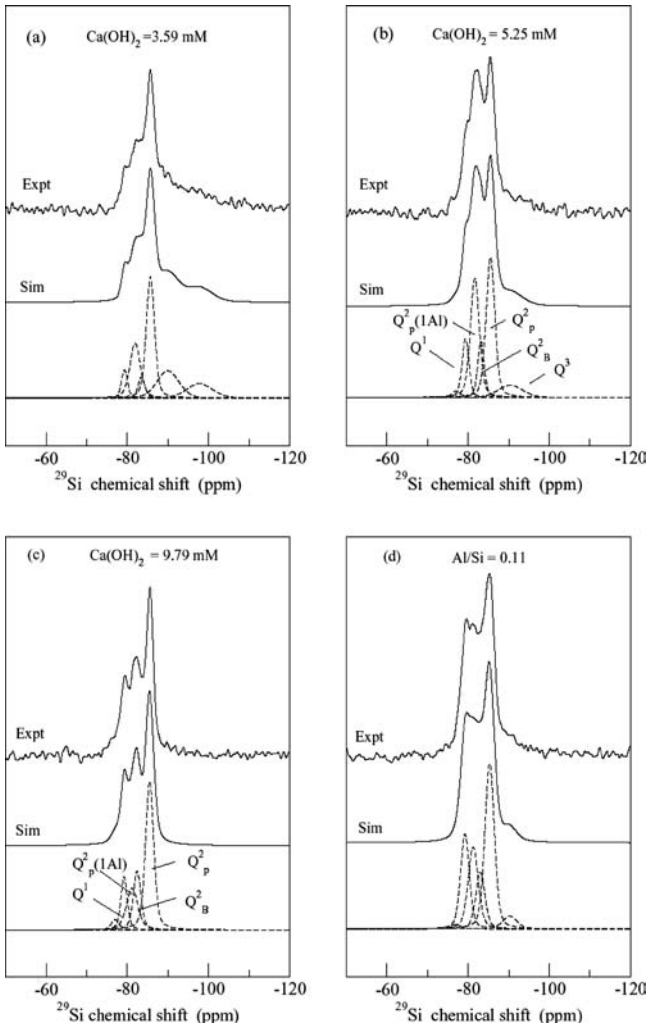

Figure 10. Comparison of the ^{29}Si MAS NMR experimental (7.05 T) and simulated spectra of C-A-S-H 0.70 (Al/Si = 0.19) equilibrated in $Ca(OH)_2$ solution. $Ca(OH)_2$ concentration: (a) 3.59 mM; (b) 5.25 mM; (c) 9.79 mM. (d): same for C-A-S-H 0.95 of Al/Si = 0.11. The simulated spectra (thin solid lines) nicely match the experimental spectra (thick solid lines) in each case. The calculated resonance peak of each silicon is also depicted (dashed lines). Each simulated spectrum in (a), (b), (c), and (d) is the sum of these resonances.

are located on the surface and in the interlayer of C-A-S-H in a role of charge-balancing of negative surface charge of the particle.[13,14,24,41] Sun et al.[24] propose that Al[V] and Al[VI]-a charge-balance Al[IV]-b. As already mentioned for the assignment of the Al resonances to structural positions, this suggestion seems to fail in view of the semiquantitative results of Table 4. Indeed, Table 4 shows that the amount of Al[IV]-b and Al[V] + Al[VI]-a are not correlated at all. For instance, there is no Al[IV]-b in the C-A-S-H 0.70 series whereas Al[V] + Al[VI]-a constitute 16−18% of the Al in C-A-S-H. On the contrary, in the C-A-S-H 0.95 series, there are 19−21% Al[IV]-b and still 16−19% Al[V]+Al[VI]-a. The expected counterions for compensation of the negative surface charge of C-A-S-H are the calcium cations. According to Tables 1 and 2, either the calcium and aluminum concentrations are of the same order of magnitude or the calcium concentration is greater than the aluminum one. Therefore, a charge compensation by Al[V] and Al[VI]-a is not likely to occur, or at least, is marginal compared to the charge compensation by calcium ions. Furthermore, no

dx.doi.org/10.1021/ic202124x | Inorg. Chem. 2012, 51, 1827−1836

amorphous Al-gel was detected in any of the samples and the semiquantitative results show that the proportion of Al[V]+Al-[VI]-a remains constant at about 18% (if the three last samples of the series in $Ca(OH)_2$ are not considered because of the great uncertainty made on the percentage of Al[VI]-a because of the presence of an AFm phase). Alternatively, one may consider these species to be closely associated with the side of the C-A-S-H particles or, in other words, with the end-chains of the aluminosilicate chains.

To test this hypothesis, one can calculate the average chain length for two (Al[V]+Al[VI]-a) (one at each ending). One has to notice that this is not a continuous chain as defined generally for C-S-H but an actual chain length taking into account the disruption because of missing bridging tetrahedra along the chain. Hence, it corresponds to the average C-A-S-H particle length within the chain direction. The average number of tetrahedra for two (Al[V]+Al[VI]-a) is equal to the sum of all the tetrahedra (Al+Si) divided by the sum Al[V]+Al[VI]-a and multiplied by 2. To be accurate, one should take into account that for each Q^1, one missing bridging tetrahedron should be considered for the calculation of the overall length. However, the Q^1 proportion is low and this correction should be ignored. Then, the average particle length (L_p) is equal to this average number of tetrahedra multiplied by the length of one dreierkett (0.73 nm) and divided by three, because one dreierkett consists of three tetrahedra (see Figure.1):

$$L_p = (\mathrm{Al[IV]} + \mathrm{Si}) \times \frac{2}{\mathrm{Al[V]} + \mathrm{Al[VI]} - a} \times \frac{0.73}{3} \quad (8)$$

Applying eq 8, one find 20 ± 3 nm which is in good agreement with the order of magnitude of C-S-H particle lengths. Nonetheless, this value is slightly lower than the size usually observed by different techniques (AFM, TEM). It has been observed elsewhere that the presence of aluminum in C_3S pastes hinders the growth of the hydrate nuclei.[42] This observation is in agreement with the C-A-S-H particle size calculated here and is consistent with an adsorption of Al[V] and Al[VI]-a on the particle sides which could hinder the particle growth.

4. CONCLUSION

An improved method has been used to decompose the ^{27}Al MAS NMR spectra allowing an accurate quantification of each type of aluminum incorporated in C-A-S-H samples. Based only on the assumption of a tobermorite-like structure to assign each of the observed resonances, the site of the aluminum could be determined. Namely, it is found that Al can substitute Si in bridging as well as in pairing positions. Al in pairing sites are observed only for Ca/(Si+Al) ratios greater than 0.95 (equivalent to 4 mmol.L^{-1} of calcium hydroxide) as predicted by ab initio calculations.[38,39]

From these results, constraints were found for an efficient decomposition of ^{29}Si MAS NMR spectra. The relative intensity of each resonance was provided by the ^{27}Al NMR results and the sample chemical composition, whereas the spectral NMR parameters were allowed to vary according to literature data. Excellent agreement between the experimental and calculated ^{29}Si NMR spectra as well as the ^{27}Al MAS NMR spectra decomposition was obtained, which strongly support the assumed C-A-S-H tobermorite-like structure.

Finally, these results suggest that penta and hexa-coordinated aluminum are adsorbed on the sides of the C-A-S-H particles.

AUTHOR INFORMATION

Corresponding Author

*E-mail: isabelle.pochard@u-bourgogne.fr.

ACKNOWLEDGMENTS

One of us (X.P.) thanks the French Research Ministry for a thesis grant. Financial support from the TGE RMN THC Fr3050 for conducting part of this research is gratefully acknowledged.

REFERENCES

(1) Ordinary Portland Cement (OPC) is a mix of clinker (~95%) and calcium sulfate (~5%); clinker results from the burning at around 1450 °C of limestone (source of CaO) and clay (source of SiO_2 and Al_2O_3). Its averaged composition is 60% tricalcium silicate, 20% dicalcium silicate, 20% of tricalcium aluminate and tetracalcium aluminoferrite. See: Taylor, H. F. W. *Cement chemistry*; Academic Press: London, U.K., 1990.

(2) Hamid, S. A. *Z. Kristallogr.* **1981**, *154*, 189.

(3) Cong, X.; Kirkpatrick, R. J. *Adv. Cem. Based Mater.* **1996**, *3*, 133–143.

(4) Klur, I.; Pollet, B.; Virlet, J.; Nonat, A. C-S-H structure evolution with calcium content by multinuclear NMR. In *Nuclear Magnetic Resonance Spectroscopy of Cement-Based Materials*; Colombet, P.; Grimmer, A.-R., Zanni, H., Sozzani, P., Eds.; Springer: Berlin, Germany, 1998; pp 119–141.

(5) Lippmaa, E.; Mägi, M.; Tarmak, M.; Wieker, W.; Grimmer, A. *Cem. Concr. Res.* **1982**, *12* (5), 597–602.

(6) Wieker, W.; Grimmer, A. R.; Winkler, A.; Mägi, M.; Tarmak, M.; Lippmaa, E. *Cem. Concr. Res.* **1982**, *12* (3), 333–339.

(7) Pellenq, R. J.-M.; Caillol, J. M.; Delville, A. *J. Phys. Chem. B* **1997**, *101*, 8584–8594.

(8) Plassard, C.; Lesniewska, E.; Pochard, I.; Nonat, A. *Ultramicroscopy* **2004**, *100* (3–4), 331–338.

(9) Plassard, C.; Lesniewska, E.; Pochard, I.; Nonat, A. *Langmuir* **2005**, *21* (16), 7263–7270.

(10) Kalousek, G. L. *J. Am. Ceram. Soc.* **1957**, *40* (3), 74–80.

(11) Engelhardt, G.; Michel, D. *High-Resolution Solid-State of Silicates and Zeolites*; Wiley: Chichester, U.K., 1987.

(12) Andersen, M. D.; Jakobsen, H. J.; Skibsted, J. *Inorg. Chem.* **2003**, *42* (7), 2280–2287.

(13) Andersen, M. D.; Jakobsen, H. J.; Skibsted, J. *Cem. Concr. Res.* **2006**, *36* (1), 3–17.

(14) Faucon, P.; Charpentier, T.; Nonat, A.; Petit, J. C. *J. Am. Chem. Soc.* **1998**, *120* (46), 12075–12082.

(15) Komarneni, S.; Roy, D. M.; Fyfe, C. A.; Kennedy, G. J. *Cem. Concr. Res.* **1987**, *17* (6), 891–895.

(16) Komarneni, S.; Roy, R.; Roy, D. M.; Fyfe, C. A.; Kennedy, G. J. *Cem. Concr. Res.* **1985**, *15* (4), 723–728.

(17) Komarneni, S.; Roy, R.; Roy, D. M.; Fyfe, C. A.; Kennedy, G. J.; Bothner-By, A. A.; Dadok, J.; Chesnick, A. S. *J. Mater. Sci.* **1985**, *20* (11), 4209–4214.

(18) Lognot, I.; Klur, I.; Nonat, A. NMR and infra-red spectroscopies of C-S-H and Al-substituted C-S-H synthetised in alkaline solutions. In *Nuclear Magnetic Resonance Spectroscopy of cement-based materials*; Colombet, P., Zanni, H., Grimmer, A., Sozzani, P., Eds.; Springer: Berlin, Germany, 1998; pp 189–196.

(19) Maeshima, T.; Noma, H.; Sakiyama, M.; Mitsuda, T. *Cem. Concr. Res.* **2003**, *33*, 1515–1523.

(20) Richardson, I. G. *Cem. Concr. Res.* **1999**, *29* (8), 1131–1147.

(21) Richardson, I. G.; Brough, A. R.; Brydson, R.; Groves, G. W.; Dobson, C. M. *J. Am. Ceram. Soc.* **1993**, *76* (9), 2285–2288.

(22) Schneider, J.; Cincotto, M. A.; Panepucci, H. *Cem. Concr. Res.* **2001**, *31* (7), 993–1001.

(23) Stade, H.; Müller, D. *Cem. Concr. Res.* **1987**, *17* (4), 553−561.
(24) Sun, G. K.; Young, J. F.; Kirkpatrick, R. J. *Cem. Concr. Res.* **2006**, *36* (1), 18−29.
(25) Wang, S. D.; Scrivener, K. L. *Cem. Concr. Res.* **2003**, *33* (5), 769−774.
(26) Andersen, M. D.; Jakobsen, H. J.; Skibsted, J. *Cem. Concr. Res.* **2004**, *34* (5), 857−868.
(27) Pardal, X.; Pochard, I.; Nonat, A. *Cem. Concr. Res.* **2009**, *39* (8), 637−643.
(28) Charpentier, T. Résonance magnétique nucléaire haute-résolution des noyaux quadrupolaires dans les solides. Ph.D. Thesis. Université Paris-sud, Orsay, France, 1998.
(29) Angeli, F.; Gaillard, M.; Jollivet, P.; Charpentier, T. *Chem. Phys. Lett.* **2007**, *440*, 324−328.
(30) Angeli, F.; Delaye, J.-M.; Charpentier, T.; Petit, J.-C.; Ghaleb, D.; Faucon, P. *Chem. Phys. Lett.* **2000**, *320* (5−6), 681−687.
(31) Neuville, D. R.; Cormier, L.; Massiot, D. *Geochim. Cosmochim. Acta* **2004**, *68* (24), 5071−5079.
(32) d'Espinose de Lacaillerie, J. B.; Fretigny, C.; Massiot, D. *J. Magn. Reson.* **2008**, *192*, 244−251.
(33) Czjzek, G. *Nucl. Instrum. Methods Phys. Res.* **1982**, *199* (1−2), 37−44.
(34) Le Caer, G.; Brand, R. A. *J. Phys.: Condens. Matter* **1998**, *10* (47), 10715−10774.
(35) d'Espinose de Lacaillerie, J.-B. Recent progress in solid-state NMR of quadrupolar nuclei: application to the characterization of hydration and sulfate attack products. In *Proceedings of the 12th International Congress in Cement Chemistry*, Montreal, Canada, 2007.
(36) Faucon, P.; Delagrave, A.; Petit, J. C.; Richet, C.; Marchand, J. M.; Zanni, H. *J. Phys. Chem. B* **1999**, *103* (37), 7796−7802.
(37) Kwan, S.; LaRosa, J.; Grutzek, M. W. *J. Am. Ceram. Soc.* **2005**, *78* (7), 1921−1926.
(38) Manzano, H.; Dolado, J. S.; Griebel, M.; Hamaekers, J. *Phys. Status Solidi A* **2008**, *204* (6), 1775−1780.
(39) Manzano, H.; Dolado, J. S.; Ayuela, A. *J. Phys. Chem. B* **2009**, *113* (9), 2832−2839.
(40) Klur, I.; Pollet, B.; Virlet, J.; Nonat, A. C-S-H structure evolution with calcium content by multinuclear NMR. In *Proceedings of the 2nd international conference on NMR-spectroscopy of cement-based materials*, Bergamo, Italy, June 1996; Colombet, P., Zanni, H., Grimmer, A., Sozzani, P., Eds.; Springer: Bergamo, 1996; p 119.
(41) Faucon, P.; Charpentier, T.; Bertrandie, D.; Nonat, A.; Virlet, J.; Petit, J. C. *Inorg. Chem.* **1998**, *37* (15), 3726−3733.
(42) Begarin, F.; Garrault, S.; Nonat, A.; Nicoleau, L. *Ann. Chim.: Sci. Matér.* **2008**, *33* (1), 251−258.